This is a preproof accepted article for *Mineralogical Magazine*
This version may be subject to change during the production process
DOI: 10.1180/mgm.2025.10095

Revision I

Plášil *et al.* Pendevilleite-(Y): A new uranyl carbonate mineral

Extending the mineralogy of U^{6+} (III.): Pendevilleite-(Y), a new uranyl carbonate mineral from Kamoto-East Open-Cut, Democratic Republic of Congo

JAKUB PLÁŠIL[1*], GWLADYS STECIUK[2], RADEK ŠKODA[3], SIMON PHILIPPO[4] AND MAEL GUENNOU[5]

[1] Institute of Physics of the CAS, Na Slovance 2, 182 00 Prague 8, Czech Republic
[2] Université de Lorraine, CNRS UMR UMR 7198, Institut Jean Lamour, 54000 Nancy, France
[3] Department of Geological Sciences, Masaryk University, Kotlářská 2, 61137 Brno, Czech Republic
[4] Section Minéralogie, Musée d'Histoire Naturelle, Rue Münster 25, Luxembourg, 2160, Luxembourg
[5] Department of Physics and Materials Science, University of Luxembourg, 41, rue du Brill - 4422 Belvaux – Luxembourg

*Corresponding author; Email: plasil@fzu.cz

Abstract
The new mineral pendevilleite-(Y) (IMA 2022-054), ideally $Mg_2Y_3Al(UO_2)_2(CO_3)_7(OH)_6(H_2O)_{16}$, was found in the famous Kamoto-East open-cut, Lualaba province, Democratic Republic of Congo and named after Jean-Marie Pendeville (1936–2002), a specialist in collecting minerals of Congo. The new mineral occurs as extremely thin blades (up to about 0.08–0.10 mm in length and only about 1 μm thick), often forming lichen-like aggregates and crusts. It is associated with kamotoite-(Y), astrocyanite-(Ce) and shabaite-(Nd), uranophane and sklodowskite. Pendevilleite-(Y) crystals are whitish or greyish-white, locally pale-bluish white. The mineral is brittle; has an irregular fracture and a Mohs hardness of about 2. Cleavage is perfect on {001}. Electron microprobe analyses provided (on the basis of 2 *apfu* U with CO_3^{2-}, H_2O derived from the structure and OH^- to keep the electroneutrality) formula $Mg_{1.78}[(Y_{1.42}Gd_{0.36}Dy_{0.33}Nd_{0.16}Er_{0.14}Sm_{0.13}Eu_{0.12}Tb_{0.05}Ho_{0.04}Yb_{0.04}Ce_{0.03}Tm_{0.03}Pr_{0.01})_{\Sigma 2.86}Ca_{0.11}Pb_{0.01}]_{\Sigma 2.98}Al_{0.88}(UO_2)_2(CO_3)_7(OH)_{5.02}(H_2O)_{16}$. Pendevilleite-(Y) is triclinic, *P*–1, a = 11.9130(3) Å, b = 13.5252(11) Å, c = 16.1531(3) Å, α = 107.052(3)°, β = 92.7765(19)°, γ = 109.676(4)° and V = 2311.5(2) Å^3 (Z = 2) at 97K. The crystal structure (dynamical refinement against 3D ED data; R_1 = 0.0948 for 1168 [$I > 3\sigma(I)$] reflections) possesses a large heteropolyhedral framework based on both finite $[(UO_2)(CO_3)_3]^{4-}$ cluster (*UTC* cluster) and a dimeric $[(UO_2)_2(CO_3)_4(OH)_2]^{6-}$ unit formed due to olation of uranyl polyhedra. There are three *M* sites in the structure, occupied by Y^{3+} and Ln^{3+}, with symmetry-related equivalents forming a polyoxometalate cluster of the general composition $[(Y,Ln)_6(OH)_8(H_2O)_4(CO_3)_4]^{2+}$. Additionally, there is one Al site in the structure (symmetrically related equivalents forming a dimer of composition $[Al_2O_2(OH)_8]^{6-}$), and two Mg sites in octahedral coordination $MgO_2(H_2O)_4$. In the sizeable channels of the framework (running parallel to **c**), there are at least eight independent partially occupied and disordered O sites of the H_2O molecules.
Keywords: pendevilleite-(Y), rare-earth elements, new mineral, crystal structure, electron diffraction, complexity

Introduction

Uranyl carbonate minerals are abundant products of hydration–oxidation weathering of uraninite (Plášil, 2014) in the presence of solutions with dissolved CO_2 that can originate from various sources (e.g., atmospheric or dissolved gangue carbonates). Due to the potentially high mobility of uranium in carbonate-bearing groundwaters, as uranyl-carbonate complexes, which are thermodynamically stable (Langmuir, 1978), those minerals are of high environmental importance. Thus, a good knowledge of the crystal chemistry and behavior of uranyl carbonate minerals is of great importance. Currently, 44 uranyl carbonates are known from nature and recognized by the IMA as minerals. Pendevilleite-(Y) is a new mineral from the Kamoto-East open-cut in Lualaba (formerly Shaba) province, Democratic Republic of Congo, Africa. It is named after Jean-Marie Pendeville (1936–2002), a school teacher and an avid mineral lover and collector. He started with mineral collecting in 1967 and expanded it during his 28-year stay in Katanga (Democratic Republic of Congo, DRC). Pendeville had a curiosity for science and a profound gift for writing. He prospected during the 1970s and 1980s on most of the local deposits together with Gilbert Gauthier, another great connoisseur of the minerals from DRC. All samples collected by J. M. Pendeville are perfectly labeled

and now stored in the collections of the Musée d'Histoire Naturelle in Luxembourg. This Congolese collection is internationally recognized as one of the finest. The mineral pocket ,with later described new minerals kamotoite-(Y), shabaite-(Nd) and astrocyanite-(Ce), was discovered by Pendeville in the early 1980s. The new mineral was found within one of the specimens he collected and labeled as an "*unknown new mineral*". The new mineral and its name have been approved by the Commission on New Minerals, Nomenclature and Classification of the International Mineralogical Association (IMA 2022-054). The Levinson suffix modifier "-(Y)" is in line with the dominance of Y over the other *REE*s in pendevilleite. The holotype specimen is deposited in the collections of the Musée d'Histoire Naturelle, Luxembourg, specimen no.VP230. Here, we report on its description, including crystal structure refinement from the 3D electron diffraction data.

Occurrence

Pendevilleite-(Y) was identified in the specimens from Kamoto-East Cu-Co deposit, exploited by the open-cut. For more detailed information about the locality we refer to the papers by Michel Deliens and Paul Piret, including descriptions of the new minerals kamotoite-(Y) (Deliens and Piret, 1986), françoisite-(Nd) (Piret *et al.*, 1988), shabaite-(Nd) (Deliens and Piret, 1989) and astrocyanite-(Ce) (Deliens and Piret, 1990). Pendevilleite-(Y) has been found in association with other uranyl carbonates that contain yttrium or lanthanoids (*Ln*): kamotoite-(Y), astrocyanite-(Ce) and shabaite-(Nd). Among non-*REE* -containing minerals, the type specimen we investigated contained uranophane and sklodowskite; the matrix consists of massive blackish pitchblende.

Physical and optical properties of pendevilleite-(Y)

Pendevilleite-(Y) occurs as extremely thin blades up to about 0.08–0.10 mm in length and only about 1 μm thick. It often forms lichen-like aggregates and crusts (Figure 1). Crystals are whitish or greyish-white, locally pale-bluish white in color (Figure 2). Pendevilleite-(Y) is non-fluorescent in both SW and LW ultraviolet light. The Mohs hardness is estimated at 2 based on tests when crystals are broken. Pendevilleite-(Y) is brittle; it has an irregular fracture. Cleavage is perfect on {001}. An experimental density could not have been determined due to a lack of available pure material. A density of 2.51 $g \cdot cm^{-3}$ is calculated for the empirical formula and 2.42 $g \cdot cm^{-3}$ for the ideal formula. No optical properties were determined due to the minimal size of the crystals and complicated intergrowths. A mean index of refraction, calculated based on Gladston-Dale equations, is $n_{GD} = 1.47$.

Chemical composition of pendevilleite-(Y)

Electron probe microanalyses (7 points on the homogeneous aggregate of crystals) were performed at the Masaryk University in Brno (CZ) on a Cameca SX-100 electron microprobe operating in WDS mode. Analytical conditions were 15 kV accelerating voltage, 10 nA beam current and 10 μm beam diameter. Such mild analytical conditions were used in order to minimize the electron beam-induced decomposition of the analyzed areas. The Raw X-ray intensities were corrected for matrix effects with a φρ(z) algorithm "X-PHI" (Merlet, 1994). Stoichiometric amounts of non-analyzed elements (C, H, O) were included in the matrix correction procedure. Inter-*REE* coincidences were corrected by empirically determined correction factors. No other elements were detected. Because insufficient material is available

to determine H_2O amounts directly, it has been calculated based on the stoichiometry derived from the structure (U = 2 *apfu*, C = 7 *apfu*, H_2O = 16 and OH calculated to keep the electroneutrality). Chemical analytical data for pendevilleite-(Y) are given in Table 1.

The empirical formula of pendevilleite-(Y) (calculated on the basis of 2 U *apfu* with CO_3^{2-}, H_2O derived from the structure and OH^- to keep the electroneutrality) is $Mg_{1.78}[(Y_{1.42}Gd_{0.36}Dy_{0.33}Nd_{0.16}Er_{0.14}Sm_{0.13}Eu_{0.12}Tb_{0.05}Ho_{0.04}Yb_{0.04}Ce_{0.03}Tm_{0.03}Pr_{0.01})_{\Sigma 2.86}Ca_{0.11}Pb_{0.01}]_{\Sigma 2.98}Al_{0.88}(UO_2)_2(CO_3)_7(OH)_{5.02}(H_2O)_{16}$. The ideal formula is $Mg_2Y_3Al(UO_2)_2(CO_3)_7(OH)_6(H_2O)_{16}$, which requires MgO 4.76, Y_2O_3 20.01, Al_2O_3 3.01, UO_3 33.80, CO_2 18.20, and H_2O 20.22, total 100 wt.%. Pendevilleite-(Y) is easily soluble in H_2O at room temperature.

Raman spectroscopy of pendevilleite-(Y)

Raman spectroscopy of pendevilleite-(Y) (Figure 2) was conducted on a Renishaw inVia micro-Raman spectrometer. Because significant fluorescence appeared using both 532 nm diode laser and a NIR (785 nm) laser, the spectrum was finally recorded using a 633 nm laser, which appeared to have the best signal-to-noise ratio (along with the lower thermal load and the consequent damages to the sample analyzed). The final spectra were obtained with a laser power of ~ 1mW through a 50× microscope objective with a numerical aperture N.A. = 0.5. The tentative assignments of the pendevilleite-(Y) spectrum were done, namely based on the papers by Čejka (1999), Koglin *et al.* (1979) and Anderson *et al.* (1980).

A broad composite band, consisting of at least three overlapping bands, appearing from ca. 3600 to 3100 cm^{-1} is attributable to stretching O–H vibrations of the molecular H_2O and OH groups. The shape of the overlapping bands in this region is characteristic of the hydrogen bonds in the structure of various strengths (bond lengths). Using the empirically derived equation of Libowitzky (1999), the calculated O···O distances of the corresponding hydrogen bonds range between ~3.0 and ~2.7 Å. A weak band, located in the spectra of both minerals at around 1562 cm^{-1} is attributable to the ν_2 (δ) (H_2O) of the molecular water. Nevertheless, those vibration bands could also be assigned to the combination bands. Usually, the ν_2 (δ) (H_2O) tends to be located towards higher energies (1600 to 1650 cm^{-1}). An asymmetric doublet (1415 and 1371 cm^{-1}) is most probably connected with the activated split doubly-degenerate ν_3 $(CO_3)^{2-}$ antisymmetric stretching vibrations of the carbonate groups. There are three sharp (lower *FWHM* than others) overlapping vibrations at 1105, 1100 and 1065 cm^{-1} that should be connected with the ν_1 $(CO_3)^{2-}$ symmetric stretching vibrations. These bands are consistent with the presence of symmetrically non-equivalent carbonate units (Koglin *et al.*, 1979; Anderson *et al.*, 1980; Čejka, 1999 and 2005, and references therein). We emphasize that there are seven independent C sites in the structure of pendevilleite-(Y) (see the structure description below). There is a weak component band at 963 cm^{-1} with a shoulder towards the lower energies; it can be ascribed to the ν_1 $(SiO_4)^{4-}$ symmetric stretching vibrations (probably of an admixture or small amount of Si in the crystals also documented by *EPMA*). A component band of the highest intensity, composed of overlapping bands at 831, 802 and 747 cm^{-1} (with pronounced shoulders), is attributable to the ν_2 (δ) $(CO_3)^{2-}$ bending vibrations and (in overlap) to the ν_1 $(UO_2)^{2+}$ symmetric stretching vibrations. Using the empirical relation of Bartlett and Cooney (1989), we can infer the corresponding U–O bond lengths from the wave numbers mentioned above (in the order given above): 1.78, 1.81,

1.87. The structure refinement provided U–O bond lengths of 1.78–1.84 Å. Therefore, all observed overlapping bands in that region may contain the contribution of the ν_1 $(UO_2)^{2+}$ symmetric stretching vibration. A doublet, 656 and 629 cm^{-1}, is attributable to ν_4 (δ) $(CO_3)^{2-}$ bending vibrations. There are several bands, those at 538, 476 and 392 cm^{-1}, which might be connected with (δ) (O–Si–O) or (δ) (Si–OH) and librations of H_2O (or with the ν_4 (δ) (SiO_4) (see, e.g., Colemenero *et al.*, 2019). Overlapping bands at 310, 239 and 215 cm^{-1} are attributable to split doubly degenerate ν_2 (δ) $(UO_2)^{2+}$ bending vibration. Bands of the lowest energies have been attributed to the lattice modes (Koglin *et al.*, 1979; Anderson *et al.*, 1980; Čejka, 1999 and 2005).

Crystallography and 3D ED data collection

The material available and its nature prevented us from obtaining powder diffraction data for pendevilleite-(Y). Therefore, we only provide the pattern calculated from crystal structure data (Table 2).

The single-crystal X-ray experiment on a Rigaku SuperNova diffractometer equipped with the microfocus Mo-source and Atlas S2 CCD detector failed due to the minimal size of the crystals, which were only poorly diffracting. Therefore, we employed 3-dimensional electron diffraction (3D ED) techniques using the transmission electron microscope (TEM) Gemmi and Lanza, 2019; Gemmi *et al.*, 2019). The new mineral's aggregate was gently crushed in a mortar in propanol and deposited on an Au-grid coated by a thin film of holey amorphous carbon. To prevent dehydration caused by the TEM high vacuum, the grid was plunged into liquid nitrogen and then transferred to the TEM using a Gatan cryo-transfer holder (Mugnaioli *et al.*, 20202; Steciuk *et al.*, 2021, 2023; Sejkora *et al.*, 2022). The 3D ED data were collected at 97K with a continuous rotation mode in an FEI Tecnai G2 TEM (acceleration voltage of 200 kV, LaB_6) equipped with a side-mounted hybrid single-electron detector ASI Cheetah M3, 512 x 512 pixels with high sensitivity and fast readout. For each selected crystal (Fig. 4), a series of non-oriented patterns are continuously collected by steps of 0.25° (data 1) and 0.25° (data 2), on all the accessible tilt ranges of the goniometer. The data collections are automated by the in-house software, including the tracking of the crystal (Plana-Ruiz *et al.*, 2020). In addition to the low-temperature experiment, low-illumination settings were used to further limit the beam-induced damage to the crystals. Continuous-rotation 3D ED data (cRED) reduction was performed using the computer program PETS2 (Palatinus *et al.*, 2019; Brázda *et al.*, 2022; Klar *et al.*, 2023). It includes the correction of geometrical and optical distortions to get accurate lattice parameters and a better integration of the reflections (Brázda *et al.*, 2022) (Figures S1 and S2). The data quality of each crystal is represented by the Rocking curve plots as well as the estimation of the crystal mosaicity, later used in the refinement (Fig. 5). The specific data processing for cRED data used in the structure solution and the refinement (with and without the dynamical approaches) is given extensively in detail by Klar *et al.* (2023). It includes introducing the overlapping virtual frames (*OVFs*) that aim to model experimental intensities from continuous rotation data by summing consecutive experimental diffraction patterns into a set of virtual frames. Each *OVF* is characterized by its angular range $\Delta\alpha_v$ covered by the virtual frame and the angular step between two virtual frames (Table 3). The result of the data reduction is a *hkl*-type file obtained from merging the two data sets (R_{int}(obs/all) = 0.1313/0.1364). This file is used in

the structure solution and the kinematical refinement. The two data sets are processed separately for the dynamical approach, where each *OVF* is considered independent (Palatinus *et al.*, 2015a, b; Klar *et al.*, 2023). The structure was solved using Superflip (Palatinus and Chapuis, 2007) implemented in Jana2020 (Petříček *et al.*, 2023) and refined using DYNGO and Jana2020.

Structure solution and refinement

At 97K, pendevilleite-Y is triclinic, with a = 11.9130(3) Å, b = 13.5252(11) Å, c = 16.1531(3) Å, α = 107.052(3)°, β = 92.7765(19)°, γ = 109.676(4)° and V = 2311.5(2) Å^3. A coverage of 92% for $\sin\theta_{full}/\lambda = 0.75$ Å^{-1} (*Laue class* -1) is reached by merging two data sets despite the strong preferential (001) orientation of the needle-like crystals on the grid. The initial model is obtained from the charge flipping algorithm in the triclinic unit cell, space group *P*–1, containing all the non-hydrogen atoms necessary for a primary interpretation. The cations present on each site were attributed according to the *EPMA* results and the coordination. The Y sites (labeled Y1, Y2 and Y3) are occupied by different proportions of Y^{3+}, Ca^{2+} and the other Ln^{3+}, where the *Ln* was set to be represented by Gd^{3+} in the case of refinement from the electron data (Gd has the average *Z* from the *Ln* distribution detected by the WDS). According to the *EPMA* results, Gd is also usually the dominant among *Ln*. Even though U for Y/*Ln* substitution is possible, it is hard to model by the refinements in the presence of several other atoms. Indeed, for the refinement, all U is assumed to be only in the two sites U1 and U2. Soft restrictions were applied in the refinement on a few cation−oxygen distances and /or angles to ensure the geometry of the carbonate groups CO_3, and the oxygen atoms of the linear uranyl groups $[O=U=O]^{2+}$ (= 1.8 Å). The initial model was refined using the dynamical theory of diffraction, which considers multiple scattering (Palatinus *et al.*, 2015a, b). The reflections of the 3D ED data involved in the refinement are filtered according to the main selection criteria *RSg* = 0.6. They are set to involve reflections that are properly covered by the experiment (Palatinus *et al.*, 2015a; Klar *et al.*, 2021). The refinement was carried out in several steps. First, the non-hydrogen atoms are refined with the occupancies of mixed sites set according to the *EPMA* results. From that refinement, hydrogen atoms were detected from the difference electrostatic potential map with isosurface levels above $2.5\sigma[\Delta V(r)]$ together with the bond valence analysis: five hydroxyl groups (O1, O5, O6, O9, O13, and O17) and eleven bonded H_2O molecules (O2, O3, O4, O7, O8, O10, O11 O12, O14, O15 and O16). The weakly-bonded H_2O molecules (labeled wat1 to wat8) tend to be disordered in the structure even at 95K. Therefore, the corresponding hydrogen sites are not visible from the difference electrostatic potential maps. All O–H distances are restricted to 1 Å and isotropic atomic displacement parameters (*ADP*s) for hydrogen are set as riding with an extension factor of 1.2. After introducing the refinement of isotropic incoherent mosaicity in the refinement (data1: 0.0917 deg; data2: 0.173 deg) *R*-values significantly dropped by 4 to 5 %, and the final refinement leads to R(obs)/wR(obs) = 0.0948/0.0895 and R(all)/wR(all) = 0.1191/0.0936 for 613 parameter and N_{obs}/N_{all} = 11686/20197 (see Table3). The residual potential map suggests that more very scarcely occupied water molecules are arranged in the channel running along the **c** axis. However, they were not added as they represent a very small contribution and the dynamical refinement of the low symmetry model with 100 atoms in the asymmetric unit cell, considering the mosaicity, took weeks to converge. Only atoms

showing clear anisotropy in their displacement parameters were anisotropically refined to reduce the refinement time. The refined formula of pendevilleite-(Y) is $AlMg_2(Y_{1.5}Gd_{1.5})_{\sum 3.00}(UO_2)_2(CO_3)_7(OH)_6(H_2O)_{10.55} \cdot 4.85H_2O$, with Gd the average *Ln* based on the microprobe analysis. The details of the data collection and refinement are presented in Table 3, and the structure is displayed in Figure 5. The atom coordinates and displacement parameters are given in Tables 4 and 5, and in the CIF file attached, selected bond distances are shown in Table 6, and a bond valence analysis is shown in Table 7.

Crystal structure of pendevilleite-(Y)

There are two U sites in the structure of pendevilleite-(Y). Both U1 and U2 sites are surrounded by eight O atoms forming squat UO_8 hexagonal bipyramids. Nevertheless, the U1 site is chelated by the three CO_3^{2-} groups to form the uranyl tricarbonate complex, $[(UO_2)(CO_3)_3]^{4-}$ (Figures 6 and 7). The U2 site is chelated differently. It is linked only to two CO_3^{2-} groups and the remaining two O atoms (O17 symmetrical equivalents) are shared with another U2-bipyramid. The O17 atom constitutes an OH group. Thus, the anionic complex comprising the U2 site is $[(UO_2)_2(CO_3)_4(OH)_2]^{6-}$ (Figure 7). Another fundamental building unit (*FBU*) of the structure of pendevilleite-(Y) is a large complex comprising six Y/*Ln* sites in coordination 9 and 8 (*M*1, *M*2, *M*3 occupied by distinct proportions of the Y^{3+}, Ln^{3+}, and Ca^{2+}). As mentioned earlier, the *Ln* has been modeled as $Gd^{3+,}$ which is usually the dominant among the *Ln* according to the *EPMA* results (and the average *Z* of the *Ln* corresponds closest one to Gd). The summary composition of this polyoxometalate cluster is $[(Y, Ln)_6(OH)_8(H_2O)_4(CO_3)_4]^{2+}$ (Figure 7). There is one Al site in the structure. Two symmetrically related equivalents result in a dimer of composition $[Al_2O_2(OH)_8(CO_3)_2{}^{2-}]^{10-}$. Two of the $(OH)^-$ are located within the shared edge of the Al-octahedra; CO_3 groups are linked monodentately (through the $O2_{C7}$ atom). There are two sites in the structure occupied by magnesium. Both Mg1, and Mg2 are bonded to six ligands in octahedral coordination, forming a dimer of $MgO_{2CO3}(H_2O)_4$ units *via* $C1O_3$ group. Two other monodentately linked carbonate groups ($C2O_3$ to Mg1 and $C6O_3$ to Mg2) (Figure 7) provide The *FBU*s are linked to form a sizeable heteropolyhedral framework structure (Figure 6), dominated by the prominent Y, *Ln*-clusters, plane-parallel to (110), cross-linked by the U2 dimers, as kind of the H-structures. In the large channels of the framework (running parallel to **c**), there are at least height-independent partially occupied and disordered O sites of the H_2O molecules. The chemical formula obtained from the structure refinement is $^{M1-}{}^{M3}(Y_{1.5}Gd_{1.5})_{\sum 3.00}AlMg_2(UO_2)_2(CO_3)_7(OH)_6(H_2O)_{10.55} \cdot 4.85H_2O$ ($Z = 2$).

Structural and chemical complexity of pendevilleite-(Y)

The structure of pendevilleite-(Y) is unique in the point of view of the structure architecture and different elements building it, and we think it is worth seeing the complexity measures of its structure. The structural complexity was determined as the Shannon information content per atom (I_G) and per unit cell ($I_{G,total}$) following the approach of Krivovichev (2012, 2013, 2014, 2016, 2017). The information-based structural complexity values were calculated using the software package TOPOS (Blatov *et al.*, 2014). The chemical complexity (Siidra *et al.*, 2014) is estimated by considering the chemical formula as a message, where symbols correspond to different chemical elements. Calculated values for the structural complexity of

pendevilleite-(Y) (including the contribution of the H-atoms, both determined and undetermined by the refinement; for the details check e.g., Gurzhiy *et al.*, 2021) are 6.781 bits/atom and 1491.90 bits/cell. Based on this value, we can consider pendevilleite-(Y) as very complex structure (Krivovichev, 2013). For comparison, we can refer to the complex sheet structure of lepersonnite-(Gd) (without the contribution of the H-atoms undetermined by the refinement; 2240.545 bits/cell)), albrechtschraufite (1161.600 bits/cell) or grimselite (140.670 bits/cell). The chemical complexity, I_{chem}, of pendevilleite-(Y) is 175.49 bits/formula. This is a particularly high value at a comparable magnitude of albrechtschraufite, $MgCa_4F_2[UO_2(CO_3)_3]_2 \cdot 17.29H_2O$ (Mereiter, 2013) (162.95 bits/formula), paddlewheelite, $MgCa_5Cu_2[(UO_2)_4(CO_3)_{12}] \cdot 33H_2O$ (Olds *et al.*, 2018) (275.27 bits/formula), or chemically-simple mineral grimselite, $K_3Na(UO_2)(CO_3)_3(H_2O)$ (Li and Burns, 2001; Plášil *et al.*, 2012) (43.58 bits/cell). The furthermost chemically complex uranyl mineral is uranyl carbonate ewingite, $Mg_8Ca_8(UO_2)_{24}(CO_3)_{30}O_4(OH)_{12}(H_2O)_{138}$ (Olds *et al.*, 2017a), with 1024.18 bits/formula.

Relation to other species

The heteropolyhedral frameworks are not unusual for U^{6+} structures, e.g., present in the mineral grimselite, $K_3Na[(UO_2)(CO_3)_3](H_2O)$ (Plášil *et al.*, 2012), or léoszilárdite, $Na_6Mg(UO_2)_2(CO_3)_6(H_2O)_6$ (Olds *et al.*, 2017b) and others (Gurzhiy *et al.*, 2021). However, pendevilleite-(Y) structure is not closely related to any other known uranyl mineral. For instance, uranyl carbonate minerals andersonite, $Na_2Ca[(UO_2)(CO_3)_3] \cdot (5+1/3)H_2O$ (Plášil and Čejka, 2015; Gurzhiy *et al.*, 2018) and grimselite, ideally $K_3Na[(UO_2)(CO_3)_3](H_2O)$ (Li and Burns, 2001; Plášil et al., 2012; Ghasizaeed *et al.*, 2018), have structures that are heteropolyhedral frameworks containing channels filled with H_2O molecules, nevertheless, both are very distinctive from pendevilleite-(Y).Albrechtschraufite $MgCa_4F_2[UO_2(CO_3)_3]_2 \cdot 17\text{-}18H_2O$ (Mereiter, 2013) can be, to some extent, considered for a comparison. There are significant cavities in the crystal structures of both minerals, filled with molecular H_2O, behaving to some extent as "zeolitic" water. Albrechtschraufite possesses a structure with U:C ratio of 1:3, organized from *FBU*s with the overall formula $MgCa_3F_2[UO_2(CO_3)_3] \cdot 8H_2O$. It consists of a uranyl tricarbonate complex associated with a large cluster of Ca^{2+}-polyhedra linked to Mg^{2+}-octahedra. By assuming that in albrechtschraufite, Ca^{2+} plays the role of *REE*s, the ratio U:C:(Mg,Al):REEs goes from 2:7:3:3 in pendevilleite-(Y) to 2:6:2:8 (1:3:1:4) in albrechtschraufite. However, the fundamental feature of the albrechtschraufite structure is a paddle wheel (Mereiter, 2013), which is not present in pendevilleite-(Y). Moreover, there is a unique feature in pendevilleite-(Y), which is a dimer of UO_8 bipyramids of the composition $U2O_{12}(OH)_2$ (olation); this arrangement, involving bonding of two H atoms within a shared edge of uranyl bipyramids, has not been observed in minerals and inorganic compounds so far (only a dimeric unit bridged by the peroxo-group, Burns, 2011; Qui and Burns, 2013). In the Strunz system, pendevilleite-(Y) belongs in class 5.E, but has a distinctive overall U:C ratio.

Given the three octahedrally coordinated *M*-sites present in pendevilleite-(Y) structure, we can expect with a high degree of certainty that there might be other new minerals. Among them, we can expect homovalent substitutions within Mg^{2+} octahedra (for instance, for Zn or Fe), or even for Cu^{2+} (that might involve some structural changes due to Jahn-Teller distorted polyhedra). To study these possible substitutions, it will be necessary to

undertake very detailed *EPMA* studies of an extended set of specimens containing Ln-uranyl-carbonates from Kamoto-East and this material is occurring only rarely nowadays.

Acknowledgements. The helpful comments of an anonymous reviewer, Vlad Gurhziy and a structure editor Peter Leverett, all helped improving the initial manuscript.. This study was supported by the CzechNanoLab Research Infrastructure supported by MEYS CR (LM2023051) (GS and JP) and an OP VVV project (Geobarr CZ.02.1.01/0.0/0.0/16_026/0008459) (RS).

Supplementary material. The supplementary material for this article can be found at .....

Competing interests. The authors declare none.

References

Bartlett, J.R. and Cooney, R.P. (1989) On the determination of uranium-oxygen bond lengths in dioxouranium(VI) compounds by Raman spectroscopy. *Journal of Molecular Structure*, **193**, 295–300.

Blatov, V.A., Shevchenko, A.P. and Proserpio, D.M. (2014) Applied topological analysis of crystal structures with the program package ToposPro. *Crystal Growth &Design*, **14**, 3576–3586.

Brázda P., Klementová, M., Krysiak, Y., and Palatinus, L. (2022) Accurate lattice parameters from 3D electron diffraction data. I. Optical distortions. *International Union of Crystallography Journal*, **9**, 1–21.

Burns, P.C. (2005) U^{6+} minerals and inorganic compounds: Insights into an expanded structural hierarchy of crystal structures. *The Canadian Mineralogist*, **43**, 1839–1894.

Burns, P.C. (2011) Nanoscale uranium-based cage clusters inspired by uranium mineralogy. *Mineralogical Magazine*, **75**, 1–25.

Čejka J. (1999) Infrared spectroscopy and thermal analysis of the uranyl minerals. Pp. 521-622. In P.C. Burns, and R.C. Ewing, Eds. *Uranium: Mineralogy, geochemistry and the environment*, 38,Mineralogical Society of America.

Colmenero, F., Plášil, J., and Sejkora, J. (2019) The layered uranyl silicate mineral uranophane-beta: crystal structure, mechanical properties, Raman spectrum and comparison with the alpha-polymorph. *Dalton Transactions*, **48**, 16722–16736.

Deliens, M., and Piret, P. (1981) La swamboite, nouveau silicate d´uranium hydrate du Shaba, Zaire. *The Canadian Mineralogist*, **19**, 553–557.

Deliens, M., and Piret, P. (1982) Bijvoetite et lepersonnite, carbonates hydrates d'uranyle et de terres rares de Shinkolobwe, Zaïre. *The Canadian Mineralogist*, **20**, 231–238.

Frost, R. L., Čejka, J., Weier, M. L., Martens, W., and Kloprogge, J. T. (2006) A Raman and infrared spectroscopic study of the uranyl silicates--weeksite, soddyite and haiweeite. *Spectrochimica Acta A*, **64**, 308–315.

Gagné, O. and Hawthorne, F.C. (2015) Comprehensive derivation of bond-valence parameters for ion pairs involving oxygen. *Acta Crystallographica*, **B71**, 562–578.

Gauthier, G., Francois, A., Deliens, M., and Piret, P. (1989) The Uranium deposits of the Shaba Region, Zaire. *The Mineralogical Record*, **20**, 265–288.

Gemmi M. and Lanza A.E. (2019) 3D electron diffraction techniques. *Acta Crystallographica Section B: Structural Science, Crystal Engineering and Materials*, **75**, 495–504.

Gemmi M., Mugnaioli E., Gorelik T.E., Kolb U., Palatinus L., Boullay P., Hovmöller S. and Abrahams J.P. (2019) 3D electron diffraction: The nanocrystallography revolution. *ACS Central Science*, **5**, 1315–1329.

Ghazisaeed, S., Majzlan, J., Plášil, J. and Kiefer, B. (2018) A simple method for the prediction of the orientation of H_2O molecules in ionic crystals. *Journal of Applied Crystallography*, **51**, 1116–1124.Gurzhiy, V.V., Krzhizhanovskaya, M.G., Izatulina, A.R., Sigmon, G.E., Krivovichev, S.V. and Burns, P.C. (2018) Structure Refinement and Thermal Stability Studies of the Uranyl Carbonate Mineral Andersonite, $Na_2Ca[(UO_2)(CO_3)_3]\cdot(5+x)H_2O$. Minerals, **8** (12), 586.

Gurzhiy, V.V., Kalashnikova, S.A., Kuporev, I.V. and Plášil, J. (2021) Crystal Chemistry and Structural Complexity of the Uranyl Carbonate Minerals and Synthetic Compounds. *Crystals*, **11**, 704.

Klar, P.B., Krysiak, Y., Xu, H., Steciuk, G., Cho, J., Zou, X., Palatinus, L. (2023) Accurate structure models and absolute configuration determination using dynamical effects in continuous-rotation 3D ED data. *Nature Chemistry*, **15**, 1–8.

Kraus, W. and Nolze, G. (1996) POWDER CELL – a program for the representation and manipulation of crystal structures and calculation of the resulting X-ray powder patterns. *Journal of Applied Crystallography*, **29**, 301–303.

Krivovichev, S.V. (2012) Topological complexity of crystal structures: quantitative approach. *Acta Crystallographica*, **A68**, 393–398.

Krivovichev, S.V. (2013) Structural complexity of minerals: information storage and processing in the mineral world. *Mineralogical Magazine*, **77**, 275–326.

Krivovichev, S.V. (2014) Which inorganic structures are the most complex? *Angewandte Chemistry, International Edition*, **53**, 654–661.

Krivovichev, S.V. (2016) Structural complexity and configurational entropy of crystals. *Acta Crystallographica*, **B72**: 274–276.

Krivovichev, S.V. (2017) Hydrogen bonding and structural complexity of the $Cu_3(AsO_4)(OH)_3$ polymorphs (clinoclase, gilmarite): a theoretical study. *Journal of Geosciences*, **62**, 79–85.

Li, Y., and Burns, P. C. (2001) The crystal structure of synthetic grimselite, $K_3Na[(UO_2)(CO_3)_3](H_2O)$. *The Canadian Mineralogist*, **39**, 1147–1151.

Libowitzky, E. (1999) Correlation of O-H stretching frequencies and O-H…O hydrogen bond lengths in minerals. *Monatshefte für Chemie*, **130**, 1047–1059.

Lussier, A.J., Lopez, R.A., and Burns, P.C. (2016) A revised and expanded structure hierarchy of natural and synthetic hexavalent uranium compounds. *The Canadian Mineralogist*, **54**, 177–283.

Mandarino, J.A. (1976) The Gladstone-Dale relationship – Part 1: derivation of new constants. *Canadian Mineralogist*, **14**, 498–502.

Mereiter, K. (2013) Description and crystal structure of albrechtschaufite, $MgCa_4F_2[UO_2(CO_3)_3]_2\cdot 17\text{-}18H_2O$. *Mineralogy and Petrology*, **10**7, 179–188.

Momma, K., and Izumi, F. (2011) VESTA 3 for three-dimensional visualization of crystal, volumetric and morphology data. *Journal of Applied Crystallography*, **44**, 1272–1276.

Mugnaioli, E., Lanza, A.E., Bortolozzi, G., Righi, L., Merlini, M., Cappello, V., Marini, L., Athanassiou, A., and Gemmi, M. (2020) Electron Diffraction on Flash-Frozen Cowlesite

Reveals the Structure of the First Two-Dimensional Natural Zeolite. *ACS Central Science*, **6**, 1578–1586.

Olds, T. A., Plášil, J., Kampf, A. R., Simonetti, A., Sadergaski, L. R., Chen, Y. S., and Burns, P. C. (2017a) Ewingite: Earth's most complex mineral. *Geology*, **45**, 1007–1010.

Olds, T. A., Sadergaski, L. R., Plášil, J., Kampf, A. R., Burns, P. C., Steele, I. M., Marty, J., Carlson, S. M., and Mills, O. P. (2017b) Leószilárdite, the first Na,Mg-containing uranyl carbonate from the Markey Mine, San Juan County, Utah, USA. *Mineralogical Magazine*, **81**, 1039–1050.

Olds, T. A., Plášil, J., Kampf, A. R., Dal Bo, F., and Burns, P. C. (2018) Paddlewheelite, a new uranyl carbonate from the Jáchymov District, Bohemia, Czech Republic. *Minerals*, **8**, 511.

Palatinus L. and Chapuis G. (2007) SUPERFLIP—a computer program for the solution of crystal structures by charge flipping in arbitrary dimensions. *Journal of Applied Crystallography*, **40**, 786–790.

Palatinus L., Corrêa C.A., Steciuk G., Jacob D., Roussel P., Boullay P., Klementová M., Gemmi M., Kopeček J., Domeneghetti M.C. and others (2015a) Structure refinement using precession electron diffraction tomography and dynamical diffraction: tests on experimental data. *Acta Crystallographica*, **B71**, 740–751.

Palatinus L., Petříček V. and Correâ C.A. (2015b) Structure refinement using precession electron diffraction tomography and dynamical diffraction: Theory and implementation. *Acta Crystallographica*, **A71**, 235–244.

Palatinus L., Brázda P., Jelínek M., Hrdá J., Steciuk G., and Klementová M. (2019) Specifics of the data processing of precession electron diffraction tomography data and their implementation in the program PETS2.0. *Acta Crystallographica*, **B75**, 512–522.

Petříček, V., Palatinus, L., Plášil, J. and Dušek, M. (2023) Jana2020 - a new version of the crystallographic computing system Jana. *Zeitschrift für Kristallographie*, **238**(7–8), 271–282.

Plášil, J. and Čejka, J. (2015) A note on the molecular water content in uranyl carbonate mineral andersonite. *Journal of Geosciences*, **60** (3) 181–187.

Plášil, J., Fejfarová, K., Skála, R., Škoda, R., Meisser, N., Hloušek, J., Císařová, I., Dušek, M., Veselovský, F., Čejka, J., Sejkora, J., and Ondruš, P. (2012) The crystal chemistry of the uranyl carbonate mineral grimselite, $(K,Na)_3Na[(UO_2)(CO_3)_3](H_2O)$, from Jáchymov, Czech Republic. *Mineralogical Magazine*, **76**, 443–453.

Plášil, J, Petříček, V., Locock, A.J., Škoda R., and Burns, P.C. (2017) The (3 + 3) commensurately modulated structure of the uranyl silicate mineral swamboite-(Nd), $Nd_{0.333}[(UO_2)(SiO_3OH)](H_2O)_{2.41}$. *Zeitschrift für Kristallographie*, **233**, 223–232.

Pouchou, J.-L., and Pichoir, F. (1991) Quantitative Analysis of Homogeneous or Stratified Microvolumes Applying the Model "PAP." Pp. 31–75 in: *Electron Probe Quantitation*. Springer US, Boston, MA.

Qui, J., and Burns, P.C. (2013) Clusters of Actinides with Oxide, Peroxide, or Hydroxide Bridges. *Chemical Reviews*, **113**, 1097−1120.

Rigaku (2023) CrysAlis CCD and CrysAlis RED. Rigaku-Oxford Diffraction Ltd, Yarnton, Oxfordshire, UK.

Siidra, O., Zenko, D.S. and Krivovichev, S.V. (2014) Structural complexity of lead silicates: crystal structure of $Pb_{21}[Si_7O_{22}]_2[Si_4O_{13}]$ and its comparison to hyttsjöite. *American Mineralogist*, **99**, 817–823.

Steciuk G., Škoda R., Rohlíček J. and Plášil J. (2020) Crystal structure of the uranyl–molybdate mineral calcurmolite $Ca[(UO_2)_3(MoO_4)_2(OH)_4](H_2O)_{\sim 5.0}$: Insights from a precession electron-diffraction tomography study. *Journal of Geosciences*, **65**, 15–25.

Steciuk G., Sejkora J., Čejka J., Plášil J. and Hloušek J. (2021) Krupičkaite, $Cu_6[AsO_3(OH)]_6 \cdot 8H_2O$, a new copper arsenate mineral from Jáchymov (Czech Republic). *Journal of Geosciences*, **66**, 37–50.

Steciuk G., Majzlan J., Rohlíček J., Škoda R., Sejkora J. and Plášil, J. (2024) Znucalite, the only known zinc uranyl carbonate: its crystal structure and environmental implications. *American Mineralogist*, **109**, 949–959.

Vincent R. and Midgley P.A. (1994) Double conical beam-rocking system for measurement of integrated electron diffraction intensities. *Ultramicroscopy*, **53**, 271–282.

FIGURE CAPTIONS

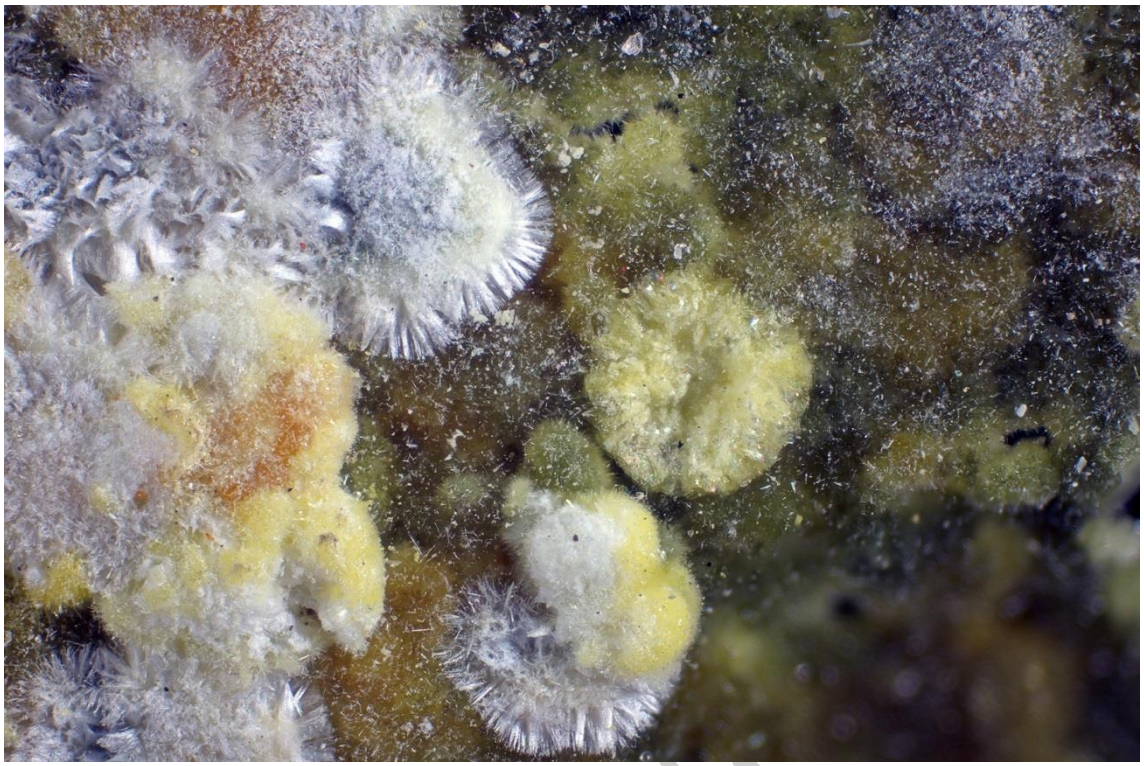

Figure 1. Whitish pendevilleite-(Y) growing along with the yellowish new unnamed mineral (most likely the yttrium analog of shabaite-(Nd)) on uranophane (greenish crystalline crust). Part of the holotype specimen used for electron diffraction experiment. Kamoto-East open pit. FOV is 2.5 mm (Photo by P. Škácha).

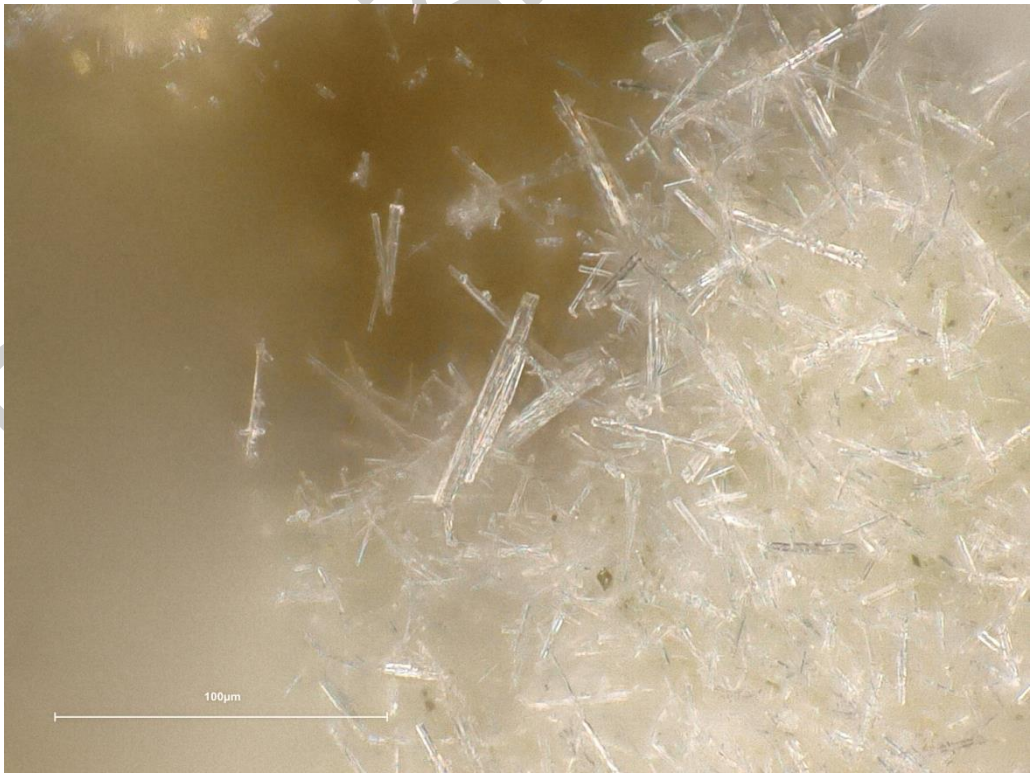

Figure 2. Detail of the pendevilleite-(Y) crystalline aggregate from the holotype specimen showing parallel intergrowths of the long-prismatic crystals. (Photo by S. Philippo).

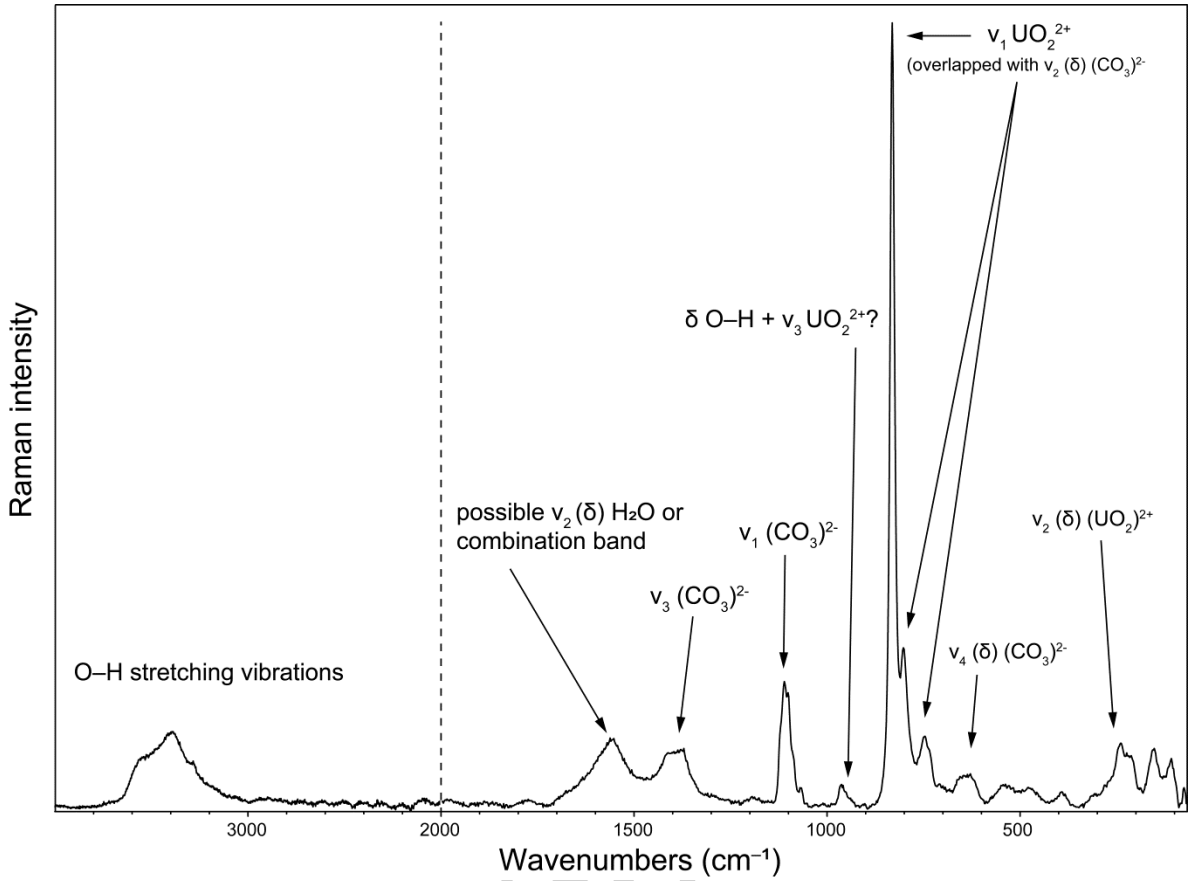

Figure 3. Raman spectrum of pendevilleite-(Y) recorded using a 633 nm diode laser.

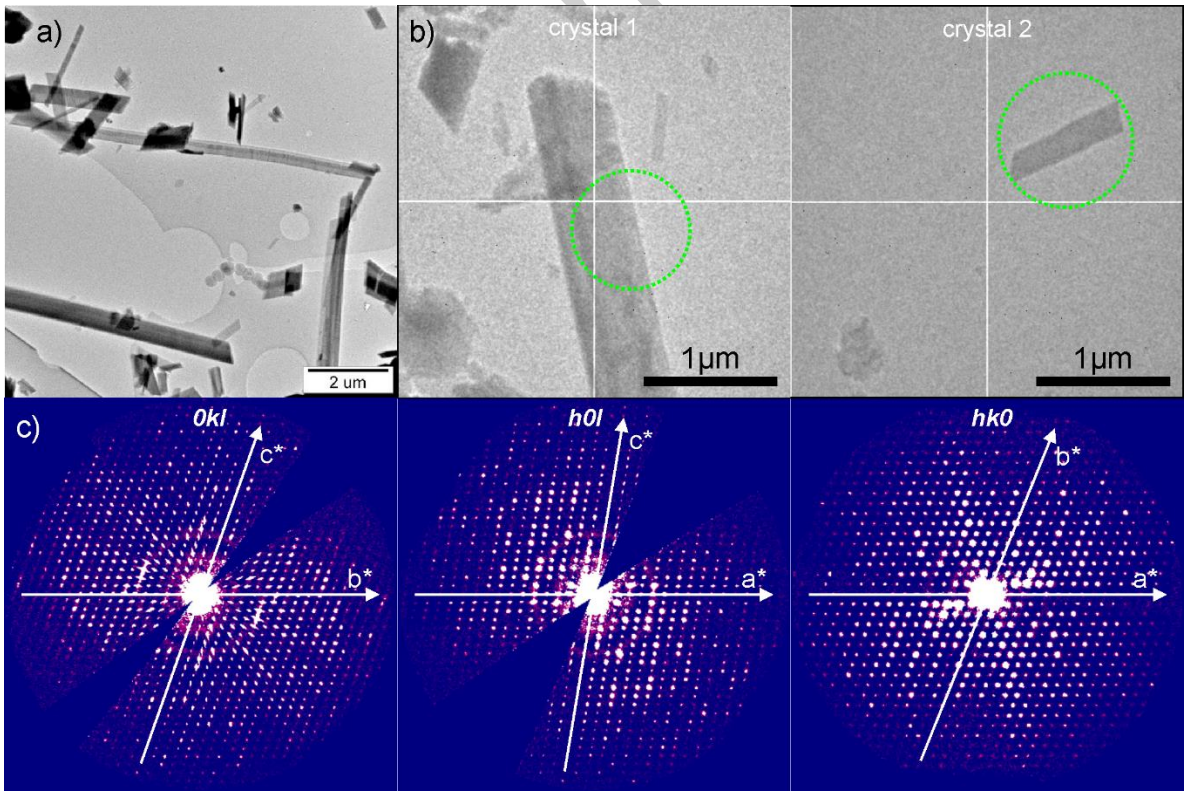

Figure 4 a) General overview of pendevilleite-(Y) crystals morphology under TEM. **B)** Crystal areas used in the 3D ED analysis (data 1 and data 2). **C)** *0kl*, *h0l* and *hk0* sections of

the reciprocal space of pendevilleite-(Y) reconstructed from the merged data set (data 1 + data 2).

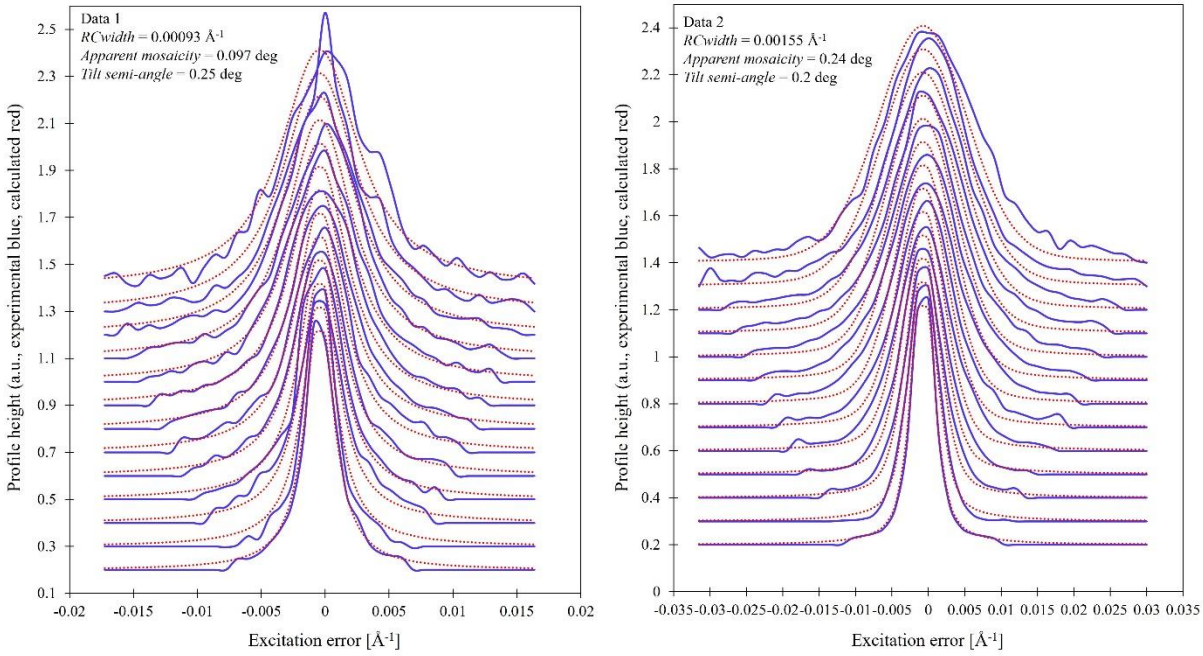

Figure 5. Plots of the rocking-curve profiles (Camel plot) of the experimental 3D ED data 1 and data 2 at 95K. The lowest blue curve is the average observed rocking curve in the range of 0.2 to 0.3 $Å^{-1}$, and the next ones are obtained by steps of 0.1 $Å^{-1}$. The red dotted curves are calculated from the *Rocking curve width*, the *apparent mosaicity*, and the tilt *semi-angle*. $I > 6*\sigma(I)$ reflections are involved in the Camel plot.

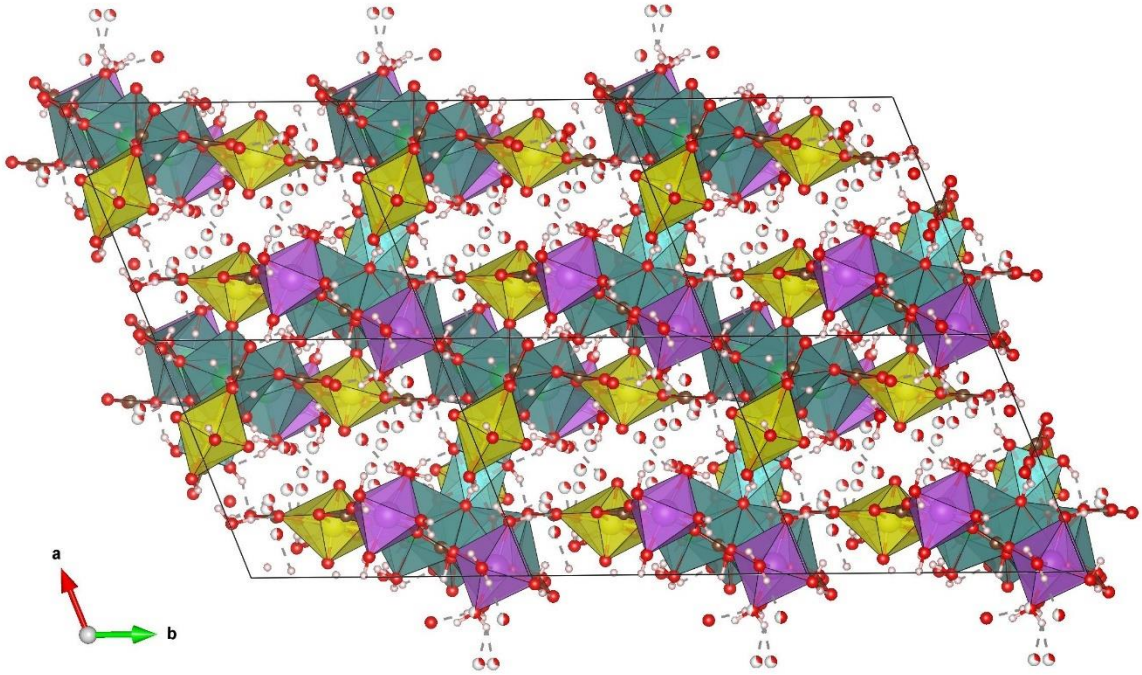

Figure 6. The structure of pendevilleite-(Y) projected down [001]. Uranyl polyhedra are yellow, Y/*REE*$^{3+}$ polyhedra green, Al-polyhedra blue, Mg-polyhedra purple and CO_3 groups brown. Black solid lines outline the unit cells.

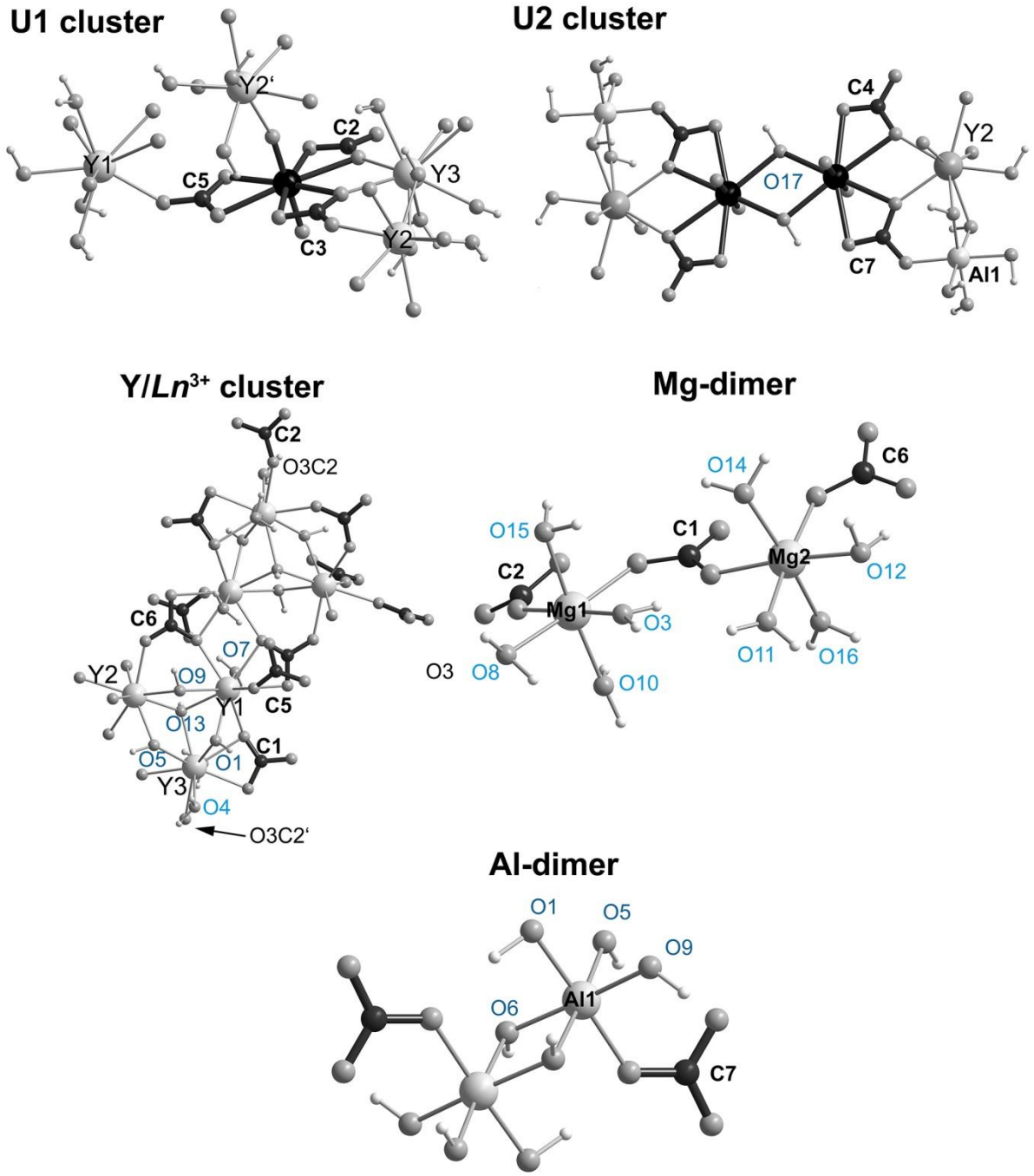

Figure 7. Cation coordination in the pendevilleite-(Y) structure. For simplicity, the Y/Ln^{3+} sites are labeled as Y1–Y3. The O atoms of the H_2O groups are given in light blue, and those of the OH^- groups in dark blue; symmetry equivalent atoms are labeled if necessary for clarity by quotation mark.

Supplementary figures

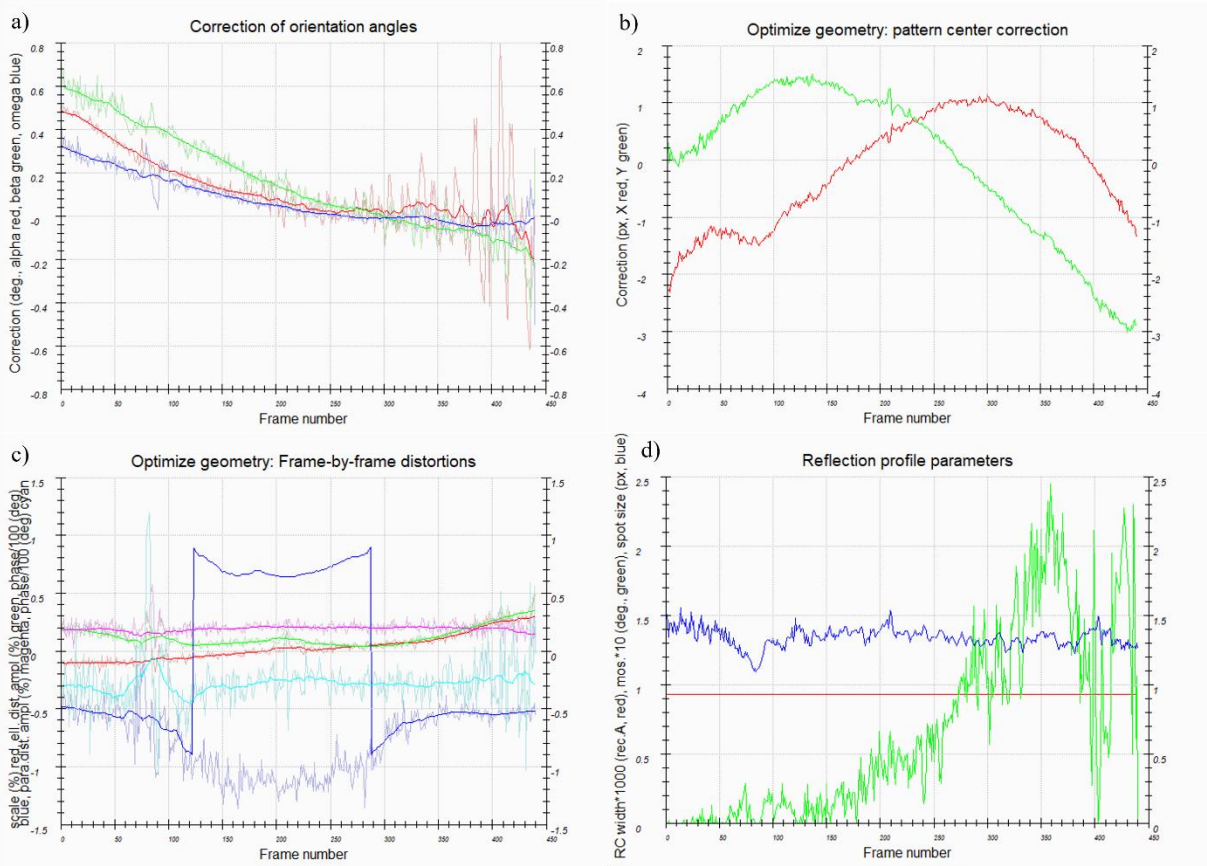

Figure S1 Geometrical optimizations of data 1 frame-by-frame. **A)** correction of the alpha-tilt, beta-tilt angles and the omega angle. Lighter curves are the initial optimized values, and the darker curves are the correction after applying a smoothing option. **B)** corrections of the coordinate *x* and *y* of the pattern center. **C)** optical distortions refinement: magnification (red), elliptical distortions amplitude (pink) and phase (dark blue), and parabolic distortions amplitude (green) and phase (light blue). The smoothing of those curves is also used to avoid outliers and noise. **D)** Refinement of the reflection profile parameters: mosaicity and the variance of the reflection size.

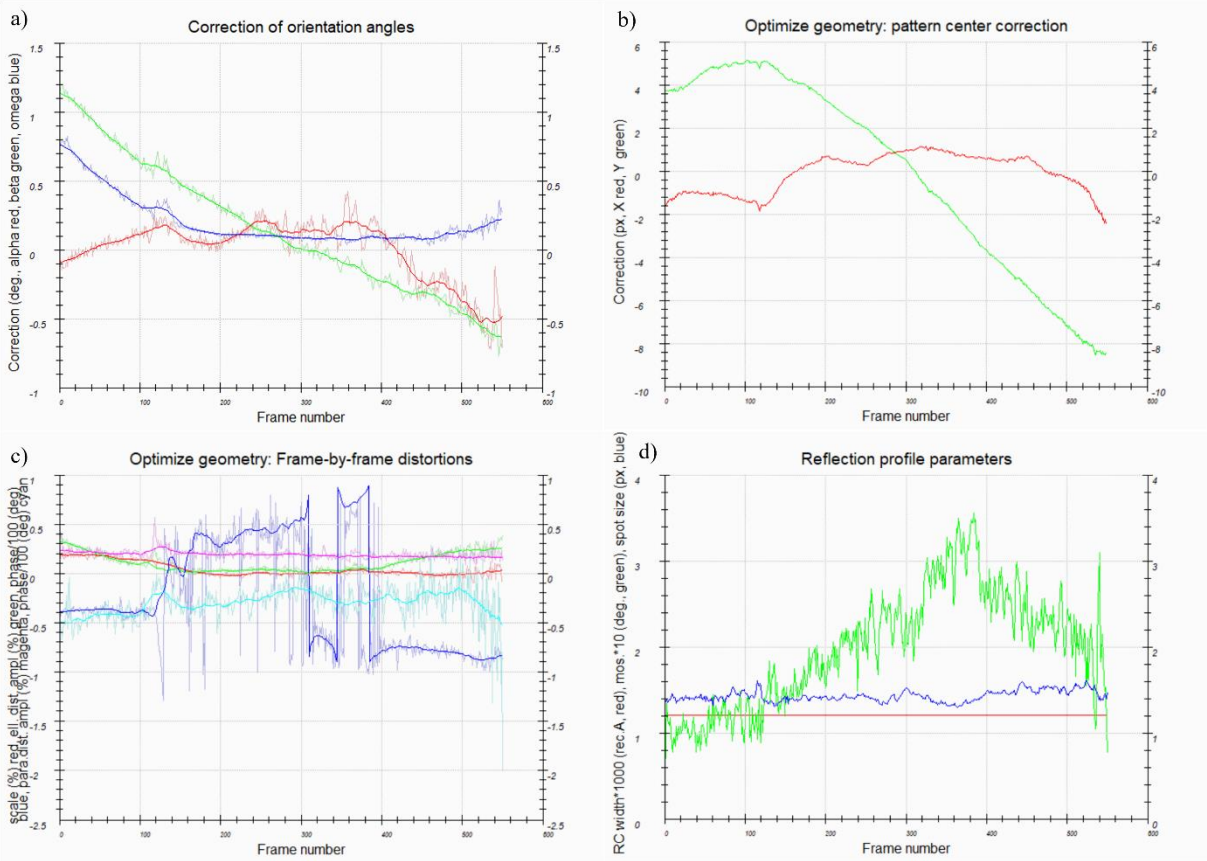

Figure S2 Geometrical optimizations of data 2 frame-by-frame. **A)** correction of the alpha-tilt, beta-tilt angles and the omega angle. Lighter curves are the initial optimized values, the darker curves are the correction after applying a smoothing option. **B)** corrections of the coordinates *x* and *y* of the pattern center. **C)** optical distortions refinement: magnification (red), elliptical distortions amplitude (pink) and phase (dark blue), and parabolic distortions amplitude (green) and phase (light blue). The smoothing of those curves is also used to avoid outliers and noise. **D)** Refinement of the reflection profile parameters: mosaicity and the variance of the reflection size.

TABLE CAPTIONS

Table 1. Chemical composition (wt.%) of pendevilleite-(Y).

Constituent	**Mean**	**Range**	**Stand. Dev.**	**Standard**
UO_3	32.50	31.97–33.23	0.48	syn. UO_2
Al_2O_3	2.54	2.28–2.67	0.22	sanidine
Y_2O_3	9.08	8.56–9.52	0.37	YPO_4
Ce_2O_3	0.25	0.22–0.30	0.03	$CePO_4$
Pr_2O_3	0.11	0.07–0.15	0.03	$PrPO_4$
Nd_2O_3	1.51	1.33–1.79	0.17	$NdPO_4$
Sm_2O_3	1.26	1.18–1.37	0.07	$SmPO_4$
Eu_2O_3	1.15	1.05–1.25	0.07	$EuPO_4$
Gd_2O_3	3.72	3.52–3.88	0.13	$GdPO_4$
Tb_2O_3	0.54	0.50–0.61	0.05	$TbPO_4$
Dy_2O_3	3.49	3.35–3.59	0.09	$DyPO_4$
Ho_2O_3	0.43	0.33–0.52	0.07	$HoPO_4$
Er_2O_3	1.47	1.41–1.51	0.04	$ErPO_4$
Tm_2O_3	0.31	0.28–0.34	0.02	$TmPO_4$
Yb_2O_3	0.45	0.43–0.48	0.02	$YbPO_4$
MgO	4.08	3.65–4.48	0.30	pyrope
CaO	0.35	0.33–0.39	0.02	wollastonite
PbO	0.08	0.03–0.13	0.04	vanadinite
CO_2*	17.50			
H_2O*	19.45			
Total	100.27			

Table 3. Theoretical powder X-ray data (d in Å) for pendevilleite-(Y) based on the structure model obtained from the 3D ED data. Only calculated lines with $I \geq 4$ are listed.

$I_{rel.calc.}$(%)	$d_{calc.}$ (Å)	h	k	l
100	**15.24**	**0**	**0**	**1**
17	12.03	0	1	0
26	11.45	0	–1	1
9	11.07	1	0	0
39	**10.23**	**–1**	**1**	**0**
4	9.74	–1	0	1
36	**8.33**	**1**	**0**	**1**
29	**8.03**	**–1**	**1**	**1**
24	7.18	–1	–1	0
19	6.82	–1	0	2
33	**6.35**	**–1**	**2**	**0**
7	5.92	–2	1	0
13	5.84	1	0	2
6	5.73	1	1	1
10	5.72	0	–2	2
6	5.54	–2	1	1
8	5.53	2	0	0
17	5.50	–2	0	1
6	4.93	–1	0	3
7	4.87	–1	–2	1
5	4.80	1	–1	3
5	4.67	–2	2	1
16	4.50	1	–3	1
11	4.45	2	1	0
7	4.35	–2	–1	2
8	4.21	0	1	3
4	3.830	2	–1	3
14	3.809	0	0	4
7	3.708	1	–2	4
9	3.702	–2	3	1
4	3.613	–3	1	2
4	3.563	–1	–3	2
4	3.539	2	–3	3
4	3.475	2	1	2
6	3.470	2	0	3
13	3.458	3	0	1
6	3.420	3	–1	2
6	3.410	–3	3	0
5	3.371	–2	–2	3
4	3.351	1	–4	2
5	3.283	–2	3	2
5	3.248	–3	0	3
4	3.217	0	–1	5
9	3.211	3	1	0
4	3.198	2	2	1
4	3.171	0	–2	5

Table 3. 3D ED data collection and structure refinement details for pendevilleite-(Y).

Refined structural formula	$AlMg_2(Y_{1.5}Gd_{1.5})_{\sum 3}(UO_2)_2(CO_3)_7(OH)_6(H_2O)_{10.55}\cdot 4.85(H_2O)$
Unit–cell parameters (3D ED):	
a [Å]	11.9130(3)
b [Å]	13.5252(11)
c [Å]	16.1531(3)
α [°]	107.052(3)
β [°]	92.7765(19)
γ [°]	109.676(4)
V [Å^3]	2311.5(2)
Z	2
Density [g·cm^{-3}]	2.5527
Space group	*P*–1
Temperature	97 K
TEM	FEI Tecnai G2 20
Radiation (wavelength)	electrons (0.0251 Å)
Δ*α*/total *α*-tilt (°)	data 1: 0.25/111 data 2: 0.2/111
OVF: $\Delta\alpha_v$*/step between OVF*(°)	data 1: 2.5/1.25 data 2: 2.6/1.40
Resolution range (θ)	0.048–1.066
Limiting Miller indices	*h*: –17→ 17, *k*: –19→18, *l*: 0 → 24
No. of independent reflections (obs/all) – kinematic (merged data)	12059/14417
R_{int} (obs/all) – kinematic	0.1313/0.1364
Redundancy	1.931
Coverage for $\sin\theta_{full}/\lambda = 0.75$ Å^{-1} (merged data)	92%
CC1/2 for $\sin\theta_{full}/\lambda = 0.75$ Å^{-1} (merged data)	96.23
Preliminary kinematical refinement (merge data)	
No. of reflections (obs/all)	10726/12179
|F(obs)-F(calc)|>15σ(F(obs))	127 rejected reflections
R, *wR* (obs); *R*, *wR* (all);	0.3457/0.4478; 0.3574/0.4504
N refined param.	237
Dynamical refinement	
RSg(max) (data 1 and data 2)	0.6
Thickness model	ribbon
apparent thicknesses data 1 and data 2	1619(12) and 1813(10) Å
No. of filtered reflections (obs) for |F(obs)-F(calc)|>10σ(F(obs))	54+123
No. of reflections (obs/all)	All: 11686/20197 Data 1: 4983/10279 Data 2: 6703/9918
R, *wR* (obs)	All: 0.0948/0.0895 Data 1: 0.0951/0.0890 Data 2: 0.0946/0.0898
R, wR (all)	All: 0.1191/0.0936 Data 1: 0.1323/0.0955

	Data 2: 0.1105/0.0924
GOF(obs)/GOF(all)	0.0243/0.0192
N all param./*N* struct. parameters	613
Incoherent mosaicity data 1/ 2 (refined) deg	0.0917 / 0.173
Residual potential (rescaled for electron)	0.996/–0.8964

Table 4. Atom coordinates and displacement parameters (Å^2) for pendevilleite-(Y).

Atom	*Occ.*	*x*	*y*	*z*	U_{eq}/U_{iso}
U1	1	1.22343(7)	0.37171(8)	0.38998(8)	0.0217(4)
U2	1	0.61352(11)	0.07192(14)	0.11801(10)	0.0619(8)
Y1/Gd1	0.5	0.90078(9)	0.09079(11)	0.56685(9)	0.0106(5)
Y2/Gd2	0.5	0.83615(10)	0.20211(12)	0.37118(11)	0.0180(6)
Y3/Gd3	0.5	0.79902(11)	0.33177(12)	0.62638(11)	0.0178(6)
Mg1	1	0.7404(6)	0.4204(6)	0.8928(4)	0.041(3)
Mg2	1	1.0349(6)	-0.1084(6)	0.1615(4)	0.048(3)
Al1	1	0.6079(3)	0.0655(3)	0.4694(3)	0.0124(16)
C1	1	0.8776(6)	0.2749(6)	0.7727(3)	0.041(5)
C2	1	0.7412(6)	0.5695(5)	0.7702(3)	0.046(5)
C3	1	0.8341(6)	0.4683(5)	0.4647(4)	0.0257(15)
C4	1	0.8647(4)	0.2496(5)	0.1563(3)	0.045(2)
C5	1	0.7445(5)	-0.1777(4)	0.5825(3)	0.0271(15)
C6	1	0.9756(5)	0.0161(4)	0.3447(3)	0.0182(13)
C7	1	0.5376(3)	0.0140(5)	0.2773(3)	0.0275(15)
O1u1	1	1.3838(3)	0.4513(5)	0.4266(5)	0.038(4)
O2u1	1	1.0602(3)	0.2967(5)	0.3598(6)	0.037(4)
O1u2	1	0.6776(9)	-0.0346(7)	0.0922(7)	0.087(4)
O2u2	1	0.5521(9)	0.1801(6)	0.1453(8)	0.087(4)
O1c1	1	0.9211(5)	0.2502(5)	0.7009(4)	0.027(3)
O2c1	1	0.8973(8)	0.2363(8)	0.8352(5)	0.058(5)
O3c1	1	0.8133(6)	0.3381(6)	0.7828(4)	0.032(3)
O1c2	1	0.7356(7)	0.6635(6)	0.7673(4)	0.043(4)
O2c2	1	0.7091(9)	0.5356(7)	0.8370(5)	0.067(6)
O3c2	1	0.7726(6)	0.5066(5)	0.7046(4)	0.029(3)
O1c3	1	0.8560(5)	0.3947(5)	0.4022(4)	0.0257(15)
O2c3	1	0.8227(5)	0.5572(5)	0.4543(5)	0.0257(15)
O3c3	1	0.8170(5)	0.4532(5)	0.5403(4)	0.0257(15)
O1c4	1	0.8248(5)	0.2141(6)	0.2207(4)	0.045(2)
O2c4	1	0.9704(5)	0.3308(6)	0.1708(4)	0.045(2)
O3c4	1	0.7978(5)	0.2081(6)	0.0796(4)	0.045(2)
O1c5	1	0.7545(5)	-0.2562(4)	0.5166(3)	0.0271(15)
O2c5	1	0.7418(5)	-0.1885(5)	0.6607(4)	0.0271(15)
O3c5	1	0.7408(5)	-0.0865(4)	0.5712(4)	0.0271(15)
O1c6	1	1.0257(5)	-0.0490(5)	0.2980(3)	0.0182(13)
O2c6	1	0.9123(5)	0.0576(5)	0.3061(3)	0.0182(13)
O3c6	1	0.9919(5)	0.0428(5)	0.4309(3)	0.0182(13)
O1c7	1	0.6443(4)	0.0861(5)	0.2781(4)	0.0275(15)
O2c7	1	0.5065(4)	-0.0019(5)	0.3508(4)	0.0275(15)

O3c7	1	0.4610(4)	-0.0393(5)	0.2043(4)	0.0275(15)
O1	1	0.7045(4)	0.1263(5)	0.5888(4)	0.0182(12)*
O2	1	0.9652(14)	0.0089(13)	0.1410(7)	0.115(10)
O3	1	0.7640(10)	0.3066(10)	0.9551(7)	0.079(6)
O4	1	0.5809(6)	0.2889(6)	0.6437(6)	0.038(3)
O5	1	0.6779(5)	0.2150(5)	0.4650(4)	0.021(3)
O6	1	0.5343(4)	-0.0846(5)	0.4806(5)	0.018(2)
O7	1	1.1236(5)	0.2067(7)	0.6121(5)	0.034(3)
O8	1	0.6572(11)	0.4920(12)	1.0020(11)	0.105(4)*
O9	1	0.7493(4)	0.0429(5)	0.4283(4)	0.0146(10*)
O10	1	0.9160(10)	0.5465(12)	0.9509(8)	0.090(7)
O11	1	1.0346(11)	-0.1575(12)	0.0227(6)	0.087(7)
O12	1	1.0061(5)	0.4790(6)	0.6953(5)	0.0293(14)
O13	1	0.9228(4)	0.2589(5)	0.5228(5)	0.019(2)
O14	1	1.2286(9)	0.0090(8)	0.1928(8)	0.086(6)
O15	1	0.5632(9)	0.2815(10)	0.8310(7)	0.084(6)
O16	0.55	0.8485(13)	-0.2464(16)	0.1461(13)	0.063(4)*
O17	1	0.4183(10)	-0.0701(13)	0.0333(8)	0.123(7)
wat1	0.325	0.711(3)	-0.1566(17)	0.2690(14)	0.069(6)*
wat1'	0.325	0.674(3)	-0.176(3)	0.289(2)	0.069(6)*
wat2	0.5	1.1826(15)	0.1554(15)	0.0717(11)	0.050(8)
wat3	1	1.1931(9)	0.4190(8)	0.7703(8)	0.094(8)
wat4	0.5	0.4221(14)	0.4018(16)	0.6457(15)	0.064(5)*
wat5	0.5	0.546(2)	0.308(2)	0.3690(17)	0.074(4)*
wat5'	0.5	0.540(2)	0.328(2)	0.4128(17)	0.074(4)*
wat6	0.175	0.443(3)	0.338(3)	0.058(3)	0.039(7)*
wat6'	0.175	0.545(3)	0.410(4)	0.144(3)	0.039(7)*
wat7	0.3	0.631(3)	-0.308(3)	0.038(3)	0.080(8)*
wat7'	0.3	0.630(3)	-0.256(3)	0.060(3)	0.080(8)*
wat8	0.25	0.614(4)	0.425(4)	0.251(4)	0.086(13)*
H1O1	1	0.6393(16)	0.084(3)	0.617(2)	0.021856*
H1O2	1	0.927(3)	0.024(6)	0.1950(10)	0.138418*
H2O2	1	1.044(4)	0.073(4)	0.154(4)	0.138418*
H1O3	1	0.825(3)	0.291(4)	0.918(2)	0.094261*
H2O3	1	0.771(5)	0.275(5)	1.004(3)	0.094261*
H1O4	1	0.520(2)	0.2161(14)	0.6050(18)	0.045203*
H2O4	1	0.549(2)	0.3462(17)	0.637(3)	0.045203*
H1O5	1	0.628(2)	0.229(3)	0.4211(17)	0.024791*
H1O6	1	0.5932(15)	-0.1074(19)	0.509(2)	0.021601*
H1O7	1	1.156(3)	0.2747(17)	0.6657(13)	0.040871*
H2O7	1	1.175(3)	0.226(3)	0.5673(15)	0.040871*
H1O8	1	0.717(3)	0.489(6)	1.046(4)	0.126455*
H2O8	1	0.576(2)	0.448(6)	1.013(5)	0.126455*
H1O9	1	0.748(3)	-0.0197(17)	0.3762(12)	0.017528*
H1O10	1	0.928(4)	0.563(3)	0.8947(14)	0.107567*
H2O10	1	0.994(2)	0.5929(9)	0.991(2)	0.107567*

H1O11	1	0.972(4)	-0.154(6)	-0.019(3)	0.104269*
H2O11	1	1.095(5)	-0.176(6)	-0.014(3)	0.104269*
H1O12	1	1.047(2)	0.5011(15)	0.6475(14)	0.035147*
H2O12	1	0.9666(15)	0.5336(13)	0.7182(10)	0.035147*
H1O13	1	1.0099(10)	0.310(2)	0.535(3)	0.023382*
H1O14	1	1.292(2)	-0.017(4)	0.211(3)	0.102711*
H2O14	1	1.245(5)	0.083(2)	0.2379(16)	0.102711*
H1O15	1	0.584(4)	0.2187(10)	0.838(2)	0.100243*
H2O15	1	0.558(5)	0.271(4)	0.7669(12)	0.100243*
H1O16	0.55	0.806(5)	-0.324(2)	0.145(3)	0.075788*
H2O16	0.55	0.785(4)	-0.227(5)	0.119(7)	0.075788*
H1O17	1	0.370(7)	-0.064(6)	0.082(4)	0.147059*

Table 5. Atom anisotropic displacement parameters ($Å^2$).

Atom	*U11*	*U22*	*U33*	*U12*	*U13*	*U23*
U1	0.0157(4)	0.0197(6)	0.0305(7)	0.0049(4)	0.0029(5)	0.0117(6)
U2	0.0437(7)	0.0916(13)	0.0308(9)	-0.0094(7)	-0.0064(7)	0.0341(11)
Y1/Gd1	0.0095(5)	0.0119(7)	0.0147(8)	0.0052(5)	0.0037(6)	0.0085(7)
Y2/Gd2	0.0131(5)	0.0202(8)	0.0207(9)	0.0030(5)	0.0027(7)	0.0103(8)
Y3/Gd3	0.0193(6)	0.0144(8)	0.0202(9)	0.0039(5)	0.0042(7)	0.0088(8)
Mg1	0.061(4)	0.041(4)	0.024(4)	0.025(3)	0.009(4)	0.007(4)
Mg2	0.074(4)	0.062(5)	0.016(3)	0.037(4)	0.005(4)	0.010(4)
Al1	0.0150(17)	0.008(2)	0.017(3)	0.0073(15)	0.007(2)	0.004(2)
C1	0.028(4)	0.054(7)	0.046(7)	0.006(4)	-0.001(5)	0.038(7)
C2	0.070(6)	0.053(7)	0.027(6)	0.029(6)	0.008(6)	0.024(7)
C3	0.0276(15)	0.0199(19)	0.035(2)	0.0092(14)	0.0116(18)	0.015(2)
C4	0.032(2)	0.066(3)	0.023(2)	0.002(2)	-0.001(2)	0.016(3)
C5	0.0232(13)	0.027(2)	0.035(2)	0.0108(14)	0.0091(18)	0.013(2)
C6	0.0253(14)	0.0171(17)	0.0110(18)	0.0105(12)	0.0010(16)	0.0001(18)
C7	0.0168(14)	0.042(2)	0.019(2)	0.0030(14)	0.0023(16)	0.013(2)
O1u1	0.027(3)	0.047(5)	0.041(5)	0.015(3)	-0.005(4)	0.016(5)
O2u1	0.021(3)	0.047(5)	0.053(6)	0.013(3)	0.009(4)	0.031(5)
O1u2	0.092(5)	0.083(6)	0.066(6)	0.001(5)	-0.009(5)	0.035(6)
O2u2	0.092(5)	0.083(6)	0.066(6)	0.001(5)	-0.009(5)	0.035(6)
O1c1	0.031(3)	0.029(4)	0.031(5)	0.016(3)	0.015(4)	0.016(4)
O2c1	0.079(6)	0.089(8)	0.034(6)	0.053(6)	0.020(6)	0.031(7)
O3c1	0.050(4)	0.042(5)	0.019(4)	0.028(4)	0.018(4)	0.018(4)
O1c2	0.075(5)	0.054(6)	0.027(5)	0.045(5)	0.018(5)	0.024(5)
O2c2	0.109(7)	0.080(8)	0.045(6)	0.062(7)	0.035(7)	0.032(7)
O3c2	0.042(4)	0.027(4)	0.029(4)	0.018(3)	0.018(4)	0.018(4)
O1c3	0.0276(15)	0.0199(19)	0.035(2)	0.0092(14)	0.0116(18)	0.015(2)
O2c3	0.0276(15)	0.0199(19)	0.035(2)	0.0092(14)	0.0116(18)	0.015(2)
O3c3	0.0276(15)	0.0199(19)	0.035(2)	0.0092(14)	0.0116(18)	0.015(2)
O1c4	0.032(2)	0.066(3)	0.023(2)	0.002(2)	-0.001(2)	0.016(3)
O2c4	0.032(2)	0.066(3)	0.023(2)	0.002(2)	-0.001(2)	0.016(3)
O3c4	0.032(2)	0.066(3)	0.023(2)	0.002(2)	-0.001(2)	0.016(3)
O1c5	0.0232(13)	0.027(2)	0.035(2)	0.0108(14)	0.0091(18)	0.013(2)
O2c5	0.0232(13)	0.027(2)	0.035(2)	0.0108(14)	0.0091(18)	0.013(2)
O3c5	0.0232(13)	0.027(2)	0.035(2)	0.0108(14)	0.0091(18)	0.013(2)
O1c6	0.0253(14)	0.0171(17)	0.0110(18)	0.0105(12)	0.0010(16)	0.0001(18)
O2c6	0.0253(14)	0.0171(17)	0.0110(18)	0.0105(12)	0.0010(16)	0.0001(18)
O3c6	0.0253(14)	0.0171(17)	0.0110(18)	0.0105(12)	0.0010(16)	0.0001(18)
O1c7	0.0168(14)	0.042(2)	0.019(2)	0.0030(14)	0.0023(16)	0.013(2)
O2c7	0.0168(14)	0.042(2)	0.019(2)	0.0030(14)	0.0023(16)	0.013(2)
O3c7	0.0168(14)	0.042(2)	0.019(2)	0.0030(14)	0.0023(16)	0.013(2)
O2	0.216(15)	0.188(15)	0.040(7)	0.162(14)	0.060(9)	0.069(10)
O3	0.133(9)	0.097(8)	0.045(6)	0.064(7)	0.041(7)	0.050(7)
O4	0.036(3)	0.023(4)	0.047(6)	0.011(3)	0.006(4)	0.000(5)

O5	0.023(3)	0.019(3)	0.028(4)	0.012(2)	0.007(3)	0.015(4)
O6	0.013(2)	0.013(3)	0.029(4)	0.005(2)	0.005(3)	0.008(3)
O7	0.024(3)	0.058(5)	0.024(5)	0.016(4)	0.007(4)	0.018(5)
O10	0.090(7)	0.113(10)	0.054(9)	0.031(7)	-0.024(8)	0.025(9)
O11	0.160(11)	0.113(9)	0.019(5)	0.097(9)	-0.002(7)	0.015(8)
O13	0.021(3)	0.016(3)	0.020(4)	0.004(2)	0.007(3)	0.006(3)
O14	0.092(7)	0.066(8)	0.085(10)	0.007(6)	0.047(8)	0.027(8)
O15	0.077(6)	0.092(8)	0.076(10)	0.029(6)	0.040(8)	0.018(8)
O17	0.090(8)	0.163(12)	0.032(7)	-0.065(8)	-0.014(7)	0.047(9)
wat2	0.081(11)	0.060(12)	0.022(9)	0.044(10)	-0.006(10)	0.012(11)
wat3	0.073(6)	0.104(10)	0.113(13)	0.036(7)	0.004(8)	0.044(11)

Table 6. Selected bond distances (Å) for pendevilleite-(Y).

U–O					
U1–O1u1	1.814(3)	U2–O1u2	1.802(11)		
U1–O2u1	1.826(3)	U2–O2u2	1.801(11)		
U1–O1c2^{i}	2.547(7)	U2–O1c4	2.692(5)		
U1–O3c2^{i}	2.545(8)	U2–O3c4	2.584(6)		
U1–O2c3^{i}	2.574(8)	U2–O1c7	2.536(6)		
U1–O3c3^{i}	2.522(7)	U2–O3c7	2.671(6)		
U1–O1c5^{ii}	2.531(7)	U2–O17	2.472(10)		
U1–O2c5^{ii}	2.553(7)	U2–O17^{iii}	2.447(14)		
<U1–O_{eq}>	2.545	<U2–O_{eq}>	2.567		
Y–O					
Y1–O1c1	2.502(6)	Y2–O2u1	2.585(4)	Y3–O1c1	2.544(8)
Y1–O3c5	2.533(5)	Y2–O1c3	2.429(7)	Y3–O3c1	2.498(7)
Y1–O1c6^{ii}	2.593(7)	Y2–O1c4	2.484(8)	Y3–O3c2	2.465(7)
Y1–O3c6	2.509(6)	Y2–O2c6	2.415(6)	Y3–O3c3	2.410(8)
Y1–O3c6^{ii}	2.549(7)	Y2–O1c7	2.411(4)	Y3–O1	2.490(6)
Y1–O1	2.561(6)	Y2–O5	2.494(7)	Y3–O4	2.514(7)
Y1–O7	2.525(6)	Y2–O9	2.513(7)	Y3–O5	2.657(6)
Y1–O9	2.580(6)	Y2–O13	2.402(7)	Y3–O12	2.533(5)
Y1–O13	2.512(8)	<Y2–O>	2.467	Y3–O13	2.489(7)
<Y1–O>	2.54			<Y3–O>	2.511
Mg–O				**Al–O**	
Mg1–O3c1	2.189(10)	Mg2–O2c1^{ii}	2.154(15)	Al1–O2c7	1.993(7)
Mg1–O2c2	2.136(14)	Mg2–O1c6	2.136(8)	Al1–O1	1.984(8)
Mg1–O3	2.152(17)	Mg2–O2	2.12(2)	Al1–O5	1.936(8)
Mg1–O8	2.201(17)	Mg2–O11	2.142(11)	Al1–O6	1.988(8)
Mg1–O10	2.153(11)	Mg2–O14	2.247(11)	Al1–O6^{iv}	1.973(7)
Mg1–O15	2.238(10)	Mg2–O16	2.315(16)	Al1–O9	1.925(7)
<Mg1–O>	2.178	<Mg2–O>	2.186	<Al1–O>	1.967
C–O					
C1–O1c1	1.293(9)	C3–O2c3	1.311(11)	C5–O3c5	1.313(9)

C1–O2c1	1.310(13)	C3–O3c3	1.311(10)	C6–O1c6	1.307(8)
C1–O3c1	1.310(12)	C4–O1c4	1.313(9)	C6–O2c6	1.310(9)
C2–O1c2	1.310(11)	C4–O2c4	1.318(7)	C6–O3c6	1.318(6)
C2–O2c2	1.317(11)	C4–O3c4	1.297(7)	C7–O1c7	1.313(6)
C2–O3c2	1.307(9)	C5–O1c5	1.308(7)	C7–O2c7	1.315(8)
C3–O1c3	1.299(9)	C5–O2c5	1.314(8)	C7–O3c7	1.303(6)

(i) –*x*+2, –*y*+1, –*z*+1; (ii) –*x*+2, –*y*, –*z*+1; (iii) –*x*+1, –*y*, –*z*; (iv) –*x*+1, –*y*, –*z*+1.

Table 7. Bond-valence analysis for pendevilleite-(Y). Values are expressed in valence units.*

	U1	U2	Y1	Y2	Y3	Mg1	Mg2	Al1	C1	C2	C3	C4	C5	C6	C7	∑		H	∑withH
O1u1	1.63															1.630	O^{2-}	-	1.63
O2u1	1.60			0.24												1.840	O^{2-}	-	1.82
O1u2		1.68														1.68	O^{2-}	-	1.68
O2u2		1.68														1.68	O^{2-}	-	1.67
O1c1			0.30		0.26				1.29							1.85	O^{2-}	-	1.85
O2c1							0.30		1.31							1.61	O^{2-}	0.15	1.76
O3c1					0.29	0.27			1.31							1.88	O^{2-}	0.03	1.91
O1c2	0.34									1.31						1.65	O^{2-}	-	1.65
O2c2						0.31				1.32						1.63	O^{2-}	-	1.63
O3c2	0.35				0.32					1.31						1.98	O^{2-}	0.05	2.03
O1c3				0.34							1.30					1.64	O^{2-}	0.10	1.74
O2c3	0.33										1.31					1.64	O^{2-}	0.06	1.7
O3c3	0.37				0.37						1.31					2.05	O^{2-}	-	2.05
O1c4		0.25		0.30								1.31				1.85	O^{2-}	-	1.85
O2c4												1.32				1.32	O^{2-}	0.13	1.45
O3c4		0.32										1.30				1.63	O^{2-}	0.26	1.89
O1c5	0.36												1.31			1.68	O^{2-}	0.16	1.84
O2c5	0.34												1.32			1.66	O^{2-}	0.13	1.79
O3c5			0.28										1.31			1.59	O^{2-}	0.11	1.7
O1c6			0.25				0.30							1.31		1.86	O^{2-}	-	1.87
O2c6				0.36										1.31		1.67	O^{2-}	0.18	1.85

O3c6			0.57											1.32		1.90	O^{2-}	-	1.9
O1c7		0.36		0.36											1.32	2.04	O^{2-}	0.02	2.06
O2c7								0.40							1.31	1.71	O^{2-}	0.1	1.81
O3c7		0.27													1.30	1.57	O^{2-}	0.11	1.68
O1			0.26		0.30			0.41								0.97	OH	0.805	1.775
O2							0.31									0.31	H_2O	1.65	1.96
O3						0.29										0.29	H_2O	1.68	1.97
O4					0.28											0.28	H_2O	1.71	1.99
O5				0.30	0.20			0.46								0.96	OH	0.83	1.79
O6								0.81								0.81	OH	0.96	1.77
O7			0.28													0.28	H_2O	1.65	1.94
O8						0.26										0.26	H_2O	1.65	1.91
O9			0.25	0.28				0.47								1.00	OH	0.83	1.83
O10						0.30										0.30	H_2O	1.65	1.95
O11							0.30									0.30	H_2O	1.65	1.95
O12					0.27											0.27	H_2O	1.65	1.93
O13			0.30	0.36	0.30											0.96	OH	0.83	1.79
O14							0.23									0.23	H_2O	1.65	1.88
O15						0.25										0.25	H_2O	1.65	1.9
O16							0.20									0.20	H_2O	1.73	1.93
O17		0.84														0.84	OH	0.83	1.65
	5.31	5.40	2.49	2.89	2.60	1.68	1.63	2.55	3.92	3.93	3.92	3.93	3.93	3.93	3.93				

* Cation–O bond valence parameters are from Gagné and Hawthorne (2015). For simplicity, the Y/Gd sites have been labeled as Y and vice versa. H atoms and non-bonded water are not included; mixed-site populations are considered in the calculations. Hydrogen-bond strengths are based on theoretical values given by Brown (2002).